Monthly Notices
of the
ROYAL ASTRONOMICAL SOCIETY

MNRAS **466,** 1061–1070 (2017)
Advance Access publication 2016 December 10

doi:10.1093/mnras/stw3121

The calibration of read-out-streak photometry in the *XMM–Newton* Optical Monitor and the construction of a bright-source catalogue

M. J. Page,[1]★ N. Chan,[1] A. A. Breeveld,[1] A. Talavera,[2] V. Yershov,[1] T. Kennedy,[1] N. P. M. Kuin,[1] B. Hancock,[1] P. J. Smith[1] and M. Carter[1]

[1]*Mullard Space Science Laboratory, University College London, Holmbury St Mary, Dorking, Surrey RH5 6NT, UK*
[2]*XMM–Newton Science Operations Centre, ESA, Villafranca del Castillo, Apartado 78, E-28691 Villanueva de la Cañada, Spain*

Accepted 2016 November 29. Received 2016 November 28; in original form 2016 September 23

ABSTRACT

The dynamic range of the *XMM–Newton* Optical Monitor (*XMM*-OM) is limited at the bright end by coincidence loss, the superposition of multiple photons in the individual frames recorded from its micro-channel-plate (MCP) intensified charge-coupled device (CCD) detector. One way to overcome this limitation is to use photons that arrive during the frame transfer of the CCD, forming vertical read-out streaks for bright sources. We calibrate these read-out streaks for photometry of bright sources observed with *XMM*-OM. The bright-source limit for read-out-streak photometry is set by the recharge time of the MCPs. For *XMM*-OM, we find that the MCP recharge time is 5.5×10^{-4} s. We determine that the effective bright limits for read-out-streak photometry with *XMM*-OM are approximately 1.5 mag brighter than the bright-source limits for normal aperture photometry in full-frame images. This translates into bright-source limits in Vega magnitudes of UVW2=7.1, UVM2=8.0, UVW1=9.4, *U*=10.5, *B*=11.5, *V*=10.2, and White=12.5 for data taken early in the mission. The limits brighten by up to 0.2 mag, depending on filter, over the course of the mission as the detector ages. The method is demonstrated by deriving UVW1 photometry for the symbiotic nova RR Telescopii, and the new photometry is used to constrain the e-folding time of its decaying ultraviolet (UV) emission. Using the read-out-streak method, we obtain photometry for 50 per cent of the missing UV source measurements in version 2.1 of the *XMM–Newton* Serendipitous UV Source Survey catalogue.

Key words: space vehicles: instruments – techniques: photometric – stars: individual: RR Tel – ultraviolet: general.

1 INTRODUCTION

The *XMM–Newton* Optical Monitor (*XMM*-OM; Mason et al. 2001) is a 30-cm Ritchey–Chrétien telescope working at ultraviolet (UV) and optical wavelengths. It is co-aligned with the X-ray mirrors on the European Space Agency's *XMM–Newton* observatory. A similar instrument, the Ultraviolet/Optical Telescope (UVOT; Roming et al. 2005) is carried on NASA's *Swift* gamma-ray-burst observatory.

The *XMM*-OM detector is a micro-channel-plate (MCP) intensified charge-coupled device (CCD; Fordham et al. 1989). Incoming photons first encounter a multi-alkali S20 photocathode, where they are converted into one or two electrons, which are then proximity focused on to a series of MCPs. The MCPs multiply the number of incoming electrons by a factor of 10^6. The resulting electron cloud then encounters a phosphor screen, which converts the signal back into photons. A tapered block of optical fibres then transmits the photons to a frame-transfer CCD with a science area of 256×256 pixels. A single photon incident on the photocathode results in a large splash of photons over several pixels of the CCD. Photon splashes are detected in individual CCD frames and centroided by the on-board electronics to a precision of one-eighth of a CCD pixel, equivalent to 0.5 arcsec on the sky.

When two or more incident photons give rise to overlapping photon splashes on the CCD during a single CCD frame, they are recorded as a single incident photon. This phenomenon is known as coincidence loss (Fordham, Moorhead & Galbraith 2000a). When the arrival rate of photons from an astronomical source is small compared to the frame rate of the CCD, coincidence loss is unimportant and the response of the instrument is linear. Coincidence loss leads to an increasingly non-linear response from the detector as the incident photon rate approaches the frame rate of the CCD. For *XMM*-OM, the non-linearity is calibrated, and photometry can

★E-mail: m.page@ucl.ac.uk

© 2016 The Authors
Published by Oxford University Press on behalf of the Royal Astronomical Society

be corrected in ground processing for incident photon rates up to 3.6 times the CCD frame rate. Photometric uncertainty becomes large as this limit is approached (Kuin & Rosen 2008). Beyond this limit, the detected photon rate saturates at approximately the frame rate of the CCD and photometry is not recoverable via the usual aperture photometry method.

One way to overcome this limitation to the dynamic range of the instrument is to use the photons that arrive during the frame transfer of the CCD. At the end of each CCD frame, the CCD image is shifted to the frame store area for read out. Photons that arrive during the frame transfer (i.e. while the image is being moved downwards towards the frame store) are displaced in the vertical direction. Bright sources therefore show vertical streaks of displaced photons, which we will refer to hereafter as read-out streaks. The frame transfer is fast enough that coincidence loss is greatly reduced in the read-out streak compared to the direct image. Page et al. (2013) showed that the read-out streaks in *Swift* UVOT images can be used for photometric measurements, and demonstrated a photometric precision of 0.1 mag. They found that the bright limit for UVOT photometry could be decreased by 2.4 mag for full-frame images using this method, with coincidence loss within the MCPs rather than the CCD dictating the bright limit for read-out-streak photometry.

In this paper, we test and calibrate read-out-streak photometry for the *XMM*-OM, before applying the method to construct a catalogue of photometry for bright sources observed with *XMM*-OM. In Section 2, we describe the basic principles of photometry using read-out streaks. In Section 3, we describe the data and methods used to calibrate the recharge time of the MCPs and verify read-out-streak photometry against sources of known brightness. The results are presented in Section 4. In Section 5, we demonstrate the technique by deriving *XMM*-OM UVW1 photometry for the symbiotic nova RR Telescopii and examining its long-term photometric evolution. In Section 6, we describe the construction of a catalogue containing photometry of sources that exceed the brightness limit of version 2.1 of the *XMM–Newton* Serendipitous UV Source Survey (*XMM*-SUSS 2.1) catalogue. Our conclusions are presented in Section 7.

Unless otherwise stated, magnitudes are given in the Vega system.

2 PRINCIPLES OF PHOTOMETRY USING READ-OUT STREAKS

The *XMM*-OM and *Swift* UVOT detectors were built to identical specifications, so the principles of read-out-streak photometry are much the same in the two instruments and the description in section 2 of Page et al. (2013) is valid for *XMM*-OM as well. However, the two instruments are operated rather differently. Whereas UVOT has only three hardware-window modes and three corresponding frame times, *XMM*-OM routinely uses a variety of hardware windows to image different parts of the field of view (see Fig. 1 for an example), and so a variety of frame times. The mathematical description that follows therefore differs from that given in Page et al. (2013) in that it is valid for any frame time, rather than for specific values.

During frame transfer, charge is shifted 290 rows downwards from the imaging portion of the CCD to the frame store area at a rate of 1 row per 6×10^{-7} s, for a total transfer time of 1.74×10^{-4} s. Photons arriving during this frame-transfer time form the read-out streak. Following Page et al. (2013), we base our read-out-streak photometry on a measurement in a 16×16 unbinned image pixel aperture, which corresponds to 2×2 CCD pixels, and therefore an effective exposure time corresponding to the transfer time of 2 CCD rows, 1.2×10^{-6} s. For a frame time $t_{\rm F}$, in which an image is accumulated and then transferred, the ratio S of the exposure time in the static image to the read-out streak is therefore

$$S = \frac{t_{\rm F} - 1.74 \times 10^{-4}}{1.2 \times 10^{-6}}. \quad (1)$$

The zero-points for read-out-streak photometry are related to the normal imaging zero-points by the ratio of equivalent exposure time S, such that

$$Z_{\rm s} = Z_{\rm i} - 2.5 \log_{10}(S), \quad (2)$$

where $Z_{\rm s}$ is the zero-point for read-out-streak photometry and $Z_{\rm i}$ is the imaging zero-point.

A complication arises in that imaging zero-points for *XMM*-OM, given in the Current Calibration File (CCF)[1] are given for 6 or 17.5-arcsec radius apertures, depending on filter (Talavera 2011), which have somewhat larger footprints than the 16×16 aperture used for the read-out-streak photometry. Therefore, we have converted the published zero-points[2] to those that would be appropriate for a 5 arcsec radius aperture using the encircled energy fractions[3] for low-count-rate sources in the CCF to match better the read-out-streak aperture, and to maintain consistency with the approach in Page et al. (2013). As the CCF does not contain a suitable encircled energy fraction calibration for the White filter, we have used the encircled energy fraction for the U filter for this purpose. The adjusted imaging zero-points, appropriate for use as $Z_{\rm i}$ in equation (2) are given in Table 1.

The dead time of the final-stage MCP is likely to limit the read-out-streak photometry at the bright end through a second stage of coincidence loss that is independent of the CCD (Fordham et al. 2000b; Page et al. 2013). The expected count rate after coincidence loss is given by equation 3 of Page et al. (2013), which is reproduced here:

$$R_{\rm o} = \frac{1 - {\rm e}^{-(S\ R_{\rm i}\ \tau_{\rm MCP})}}{S\ \tau_{\rm MCP}}, \quad (3)$$

where $R_{\rm o}$ is the count rate observed from the read-out streak in a 16×16-pixel aperture, $R_{\rm i}$ is incident count rate that would be observed if there was no coincidence loss in the MCP, and $\tau_{\rm MCP}$ is the MCP recharge time-scale.

Rearranging equation (3), we obtain the following equation for $R_{\rm i}$:

$$R_{\rm i} = -\frac{\log_{\rm e}(1.0 - (S\ R_{\rm o}\ \tau_{\rm MCP}))}{S\ \tau_{\rm MCP}}. \quad (4)$$

The gradual decline in *XMM*-OM sensitivity with time will affect read-out-streak photometry in the same way as it affects normal aperture photometry. Therefore, $R_{\rm i}$ should be corrected by the time-dependent sensitivity correction,[4] which is contained within the CCF. If C is the time-dependent sensitivity correction factor and $R_{\rm c}$ is the read-out-streak count rate after correction, then

$$R_{\rm c} = C \times R_{\rm i} \quad (5)$$

and $R_{\rm c}$ can be used with the appropriate zero-point $Z_{\rm s}$ to obtain a magnitude m:

$$m = -2.5 \log_{10}(R_{\rm c}) + Z_{\rm s} \quad (6)$$

[1] http://www.mssl.ucl.ac.uk/www_astro/XMM-OM-SUSS/suss2_1/
[2] Calibration file OM_COLOURTRANS_0010.CCF.
[3] Calibration file OM_PSF1DRB_0010.CCF.
[4] Calibration file OM_PHOTTONAT_0004.CCF.

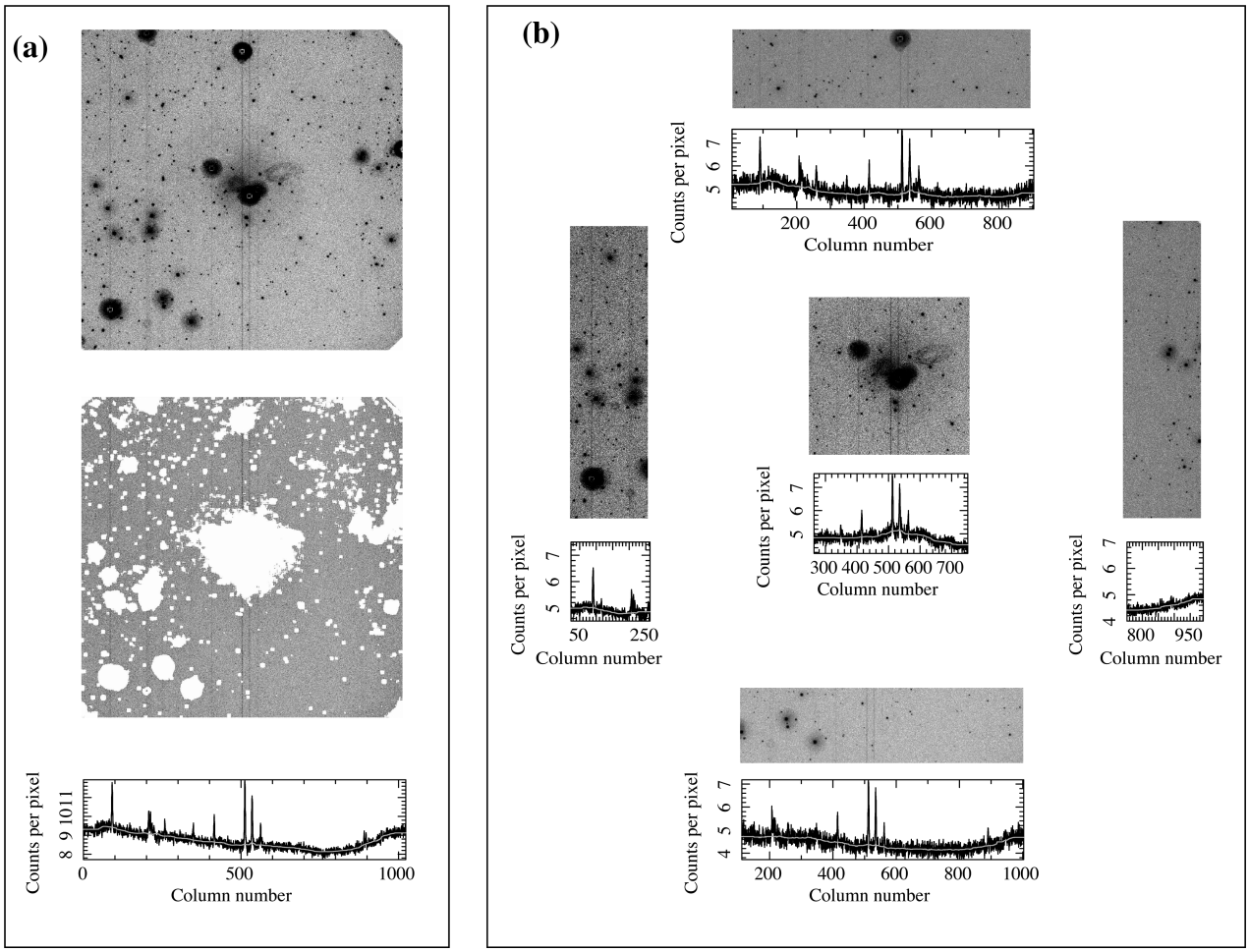

Figure 1. Illustration of the read-out-streak and measurement process. Panel (a) shows a full-frame image before (top) and after (middle) masking of sources. In the graph at the bottom of panel (a), the black line shows the mean counts per pixel for each column of the masked image, while the grey line shows the background estimate (see Section 3.3). The read-out streaks appear as positive spikes above the background estimate. Panel (b) shows the same field imaged in the default imaging mode (also known as 'Rudi-5' mode) in which five separate images are taken to cover the field of view, together with the counts per column and background levels for each of the five images after masking.

Table 1. *XMM*-OM imaging Vega and AB zero-points scaled to a 5-arcsec radius aperture, suitable for use as Z_i in equation (2). For the White filter, we do not provide an AB zero-point because the CCF does not contain an AB zero-point for this filter.

Filter	Vega zero-point (mag)	AB zero-point (mag)
V	17.9501	17.9098
B	19.2481	19.0629
U	18.2408	19.1705
UVW1	17.1247	18.4871
UVM2	15.7004	17.3400
UVW2	14.8200	16.5252
White	20.2370	–

3 METHODS

3.1 Input catalogue and data set

In order to calibrate and qualify read-out-streak photometry for *XMM*-OM, we must measure the read-out streaks for sources of known (or predictable) brightness in one or more *XMM*-OM photometric passbands. The most reliable and widely available photometry for stars in the magnitude range relevant for read-out-streak photometry comes from the *Tycho*-2 catalogue (ESA 1997; Høg et al. 2000). *Tycho*-2 is a catalogue of stars for which photometry was recorded by the star mapper on the European Space Agency (ESA)'s *Hipparcos* satellite. *Tycho*-2 contains photometry in two bandpasses, V_T and B_T, which cover similar but not identical wavelength ranges as the *V* and *B* bands of *XMM*-OM.

In order to obtain a suitable data set, we correlated the *XMM*-SUSS 2.1 catalogue (Page et al. 2012)[5] with the *Tycho*-2 catalogue using a matching radius of 5 arcsec. In order to avoid crowded fields, we excluded matches within 20 deg of the Galactic plane. Matches were restricted to *Tycho*-2 sources with $V_T \leq 12$ mag, which have the most reliable *Tycho*-2 photometry. Transformation from *Tycho*-2 photometry to photometric systems similar to that of the *XMM*-OM is known to be less reliable for stars of spectral type M than for stars of earlier spectral type (ESA 1997; Page et al. 2013). It is difficult to differentiate M stars from earlier types using

[5] Updated information with respect to Page et al. (2012) relevant to version 2.1 of the *XMM*-SUSS is available at http://www.ucl.ac.uk/mssl/astro/space_missions/xmm-newton/xmm-suss2.

Tycho-2 $B_T - V_T$ colour, so we obtained near-infrared photometry by cross-correlating our sample with the Two Micron All Sky Survey (Skrutskie et al. 2006). Stars with $V_T - J > 3.0$ were then excluded from our catalogue because they are likely to be M stars. It simplifies the analysis to have a common frame time for all observations, so the data set was further restricted to *Tycho*-2 stars observed with full-frame *XMM*-OM observations, which have a frame time of 11.0388 ms. For stars that have been repeatedly observed by *XMM–Newton*, for each filter we used data from only a single *XMM–Newton* pointing. Hence, each star is represented by a single *XMM*-OM measurement in any filter, and the level of systematic error derived from the analysis will be representative of the systematics occurring in individual *XMM–Newton* pointings.

3.2 Transformation from the *Tycho*-2 to *XMM*-OM photometric system

To derive the transformation between *Tycho*-2 and *XMM*-OM photometric systems, we generated synthetic photometry for the Pickles (1998) atlas of stellar spectra in both systems. Transformations involving the *Tycho*-2 system are known to have a much larger scatter for M-type stars than for earlier types (ESA 1997; Page et al. 2013), and hence M star templates were not used for the synthetic photometry. The colours relating V and B in the *XMM*-OM system to V_T and B_T in the *Tycho*-2 system from the synthetic photometry are shown in Fig. 2.

The transformations between *Tycho* and *XMM*-OM are approximately linear over a significant range in $B_T - V_T$. The following transformations were obtained from least-squared fits to the synthetic photometry:

$$V = V_T - 0.002 - 0.074(B_T - V_T) \quad (7)$$

for $0 < (B_T - V_T) < 2$ and

$$B = B_T + 0.0672 - 0.2538(B_T - V_T) \quad (8)$$

for $0.4 < (B_T - V_T) < 2$. These relations are shown as solid lines in Fig. 2. The rms scatter in $V_T - v$ and $B_T - b$ about these relations are 0.006 and 0.009 mag, respectively.

3.3 Measurement of the read-out streaks

Read-out streaks were measured from raw *XMM*-OM images after correction for modulo-8 noise by the standard *XMM–Newton* pipeline processing.

Prior to measuring the streaks, sources and bad pixels were masked from the images. The first step was to mask bad pixels identified in the standard *XMM*-OM calibration file[6] within the CCF. Next, bright sources with count rates >40 counts s^{-1} were identified via a sliding-box search; bright sources are surrounded by dark regions produced by coincidence loss, so a 24 arcsec radius region was masked around each bright source. Masking of other sources was carried out on a column by column basis to prevent the read-out streaks themselves being detected as sources. First, for each column, the median brightness was calculated and any pixels brighter than the median by more than 3σ, or by more than three counts if the median of the column is ≤ 1, were flagged. Next, the column is smoothed with a 10 pixel box-car filter to aid the detection of faint sources, and again any pixel that is brighter than the median of the column by more than 3σ, or three counts if the median of the column is ≤ 1, was flagged. All pixels flagged in either step were then masked.

[6] Calibration file OM_BADPIX_0005.CCF.

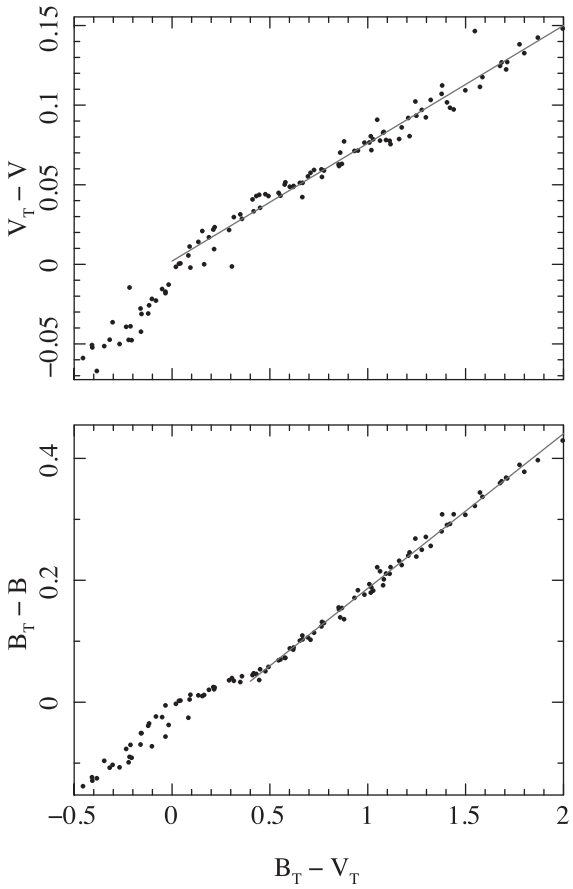

Figure 2. Relations between *XMM*-OM V and *Tycho*-2 V_T magnitudes and between *XMM*-OM B and *Tycho*-2 B_T magnitudes, with respect to *Tycho*-2 $B_T - V_T$ colour. The black dots correspond to synthetic photometry for stars in the Pickles (1998) stellar library. The grey lines correspond to the linear relations adopted in this work for transformations between *Tycho*-2 and *XMM*-OM systems.

Next, for each column the mean value for all non-masked pixels was computed, and used to populate a single row of column brightness values. For each pixel in this one-dimensional row, the median of the pixel values within a 128 unbinned-pixel-wide box was used to define a background, and read-out streaks were then detected using a sliding 16 unbinned-pixel cell. Examples showing the column brightness and corresponding background for images taken in full-frame mode and the default imaging mode are shown in Fig. 1. For streaks detected at $>6\sigma$, the count rate was summed over the 16-pixel interval and background subtracted. Next, the count rates were multiplied by a factor of 16 to scale them from the equivalent of a single-pixel slice of the aperture to the full 16 × 16-pixel aperture. Finally, the count rates of the read-out streaks were corrected for the time-dependent sensitivity degradation of the *XMM*-OM (Talavera 2011).

The procedure just described differs from that described in section 3.2 of Page et al. (2013) for UVOT read-out streaks only in two aspects. First, no bad-pixel mask was employed in Page et al. (2013), but in this work we have found that masking the bad pixels improves the read-out-streak detection and photometry towards the edges of the images. Secondly, whereas corrections for large-scale

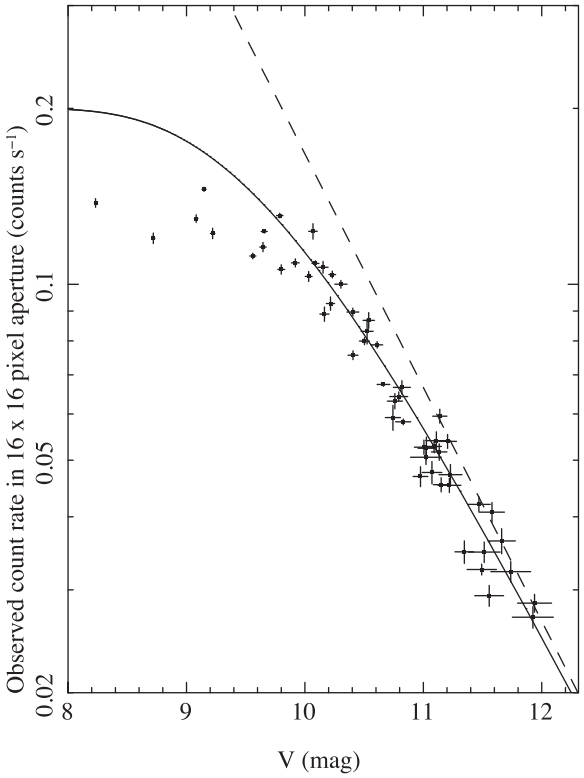

Figure 3. Data points show the observed read-out-streak count rates in 16 × 16-pixel apertures (equivalent to R_o in equations 3 and 4) of *Tycho*-2 stars against *XMM*-OM *V* magnitude, derived from *Tycho*-2 photometry (equation 7). The dashed line shows the expected relationship if there were no coincidence loss in the MCPs, (i.e. if $R_i = R_o$). The solid line shows the expected relationship for an MCP recharge time $\tau_{MCP} = 5.5 \times 10^{-4}$ s, as derived in Section 4.

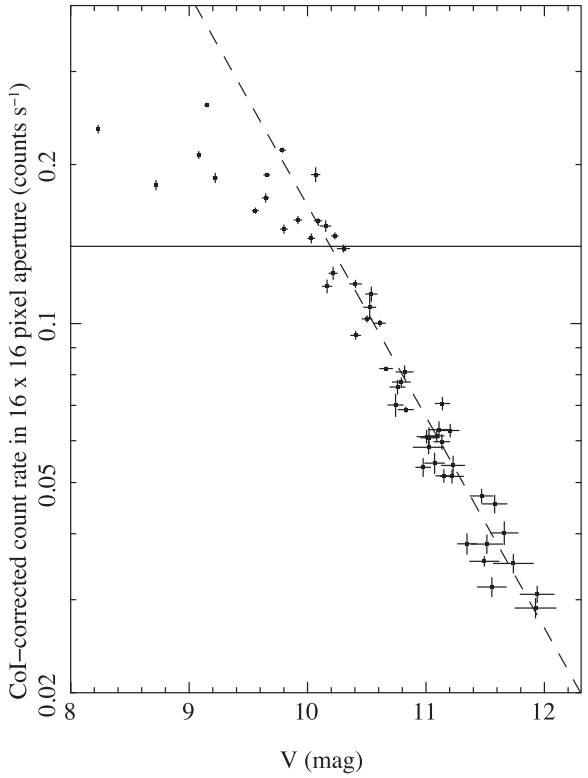

Figure 4. Data points show the read-out-streak count rates in 16 × 16-pixel apertures of *Tycho*-2 stars in full-frame *XMM*-OM *V*-band images after correction for coincidence loss in the MCPs (equivalent to R_i in equations 3 and 4) against *XMM*-OM *V* magnitude, derived from *Tycho*-2 photometry (equation 7). The dashed line shows the expected relationship. The solid line shows a count rate of 0.14 counts s^{-1}, below which saturation effects are not important.

sensitivity variations of UVOT were applied in Page et al. (2013), there are no such corrections for *XMM*-OM.

Where multiple full-frame exposures have been taken through the same filter in the same *XMM–Newton* observation, the read-out-streak count rates were averaged. To ensure good quality photometry for the calibration, only measurements with a signal-to-noise ratio >20 were used. There are suitable measurements for 54 stars in the *V* band and 25 stars in the *B* band.

4 RESULTS

Fig. 3 shows the count rates measured in the read-out streaks against the predicted *V* magnitudes for the *Tycho*-2 stars. The dashed line shows the predicted relationship if there were no coincidence loss within the MCPs. While the measurements approach the dashed line at faint magnitudes, the difference is large at bright magnitudes, implying that, as expected, coincidence loss in the *XMM*-OM MCPs has a significant effect on the read-out streaks of bright sources. For sources brighter than $v = 10$ mag, the read-out-streak count rate shows only a weak dependence on source magnitude. To determine the MCP recharge time-scale, τ_{MCP}, we performed a χ^2 fit in which the observed count rate is related to the incident count rate according to equation (3) to the sources fainter than $V = 10$ mag in Fig. 3. We obtain a best-fitting $\tau_{MCP} = 5.5 \pm 0.1 \times 10^{-4}$ s.

The solid line in Fig. 3 shows the expected relation between *V* magnitude and count rate for the best-fitting value of τ_{MCP}. The model reproduces the data well up to the $V = 10$-mag bright limit of the fit, but for $V < 10$ mag the model and data diverge systematically towards brighter magnitudes, with the count rates falling below the expectations of the model for all sources with $V < 9.8$ mag. Furthermore, at the brightest magnitudes, the statistical uncertainties in the measurements are small, and therefore we would expect the scatter in the measured count rates to diminish towards bright magnitudes as the count rates converge towards the saturation limit. Instead, the small number of measurements at $V < 9.5$ mag exhibit significant scatter. This scatter, combined with the relatively flat relation between count rate and magnitude, precludes the use of read-out streaks for photometric measurement at the brightest magnitudes. Similar deviations from the model predictions at bright fluxes were observed by Page et al. (2013) in the *Swift* UVOT, who suggested that charge bleeding in the CCD, or positional dependences in electron mobility in the MCPs, might be responsible. It is interesting to note that $\tau_{MCP} = 5.5 \times 10^{-4}$ s is significantly longer than that found by Page et al. (2013) for *Swift* UVOT, such that coincidence loss in the MCPs becomes significant at a lower count rate in *XMM*-OM than in UVOT. The bright limit beyond which the data deviate from the coincidence-loss model is also shifted to fainter magnitudes in *XMM*-OM compared to UVOT. This finding suggests that it is the behaviour of the MCPs, rather than charge bleeding in the CCD, that is responsible for the break-down of the model at bright magnitudes.

Correcting the observed read-out-streak count rates for coincidence loss in the MCPs using equation (4) and $\tau_{MCP} = 5.5 \times 10^{-4}$ s, we obtain Fig. 4. A close correlation is seen between count rate and magnitude for coincidence-loss-corrected count rates $R_i < 0.14$

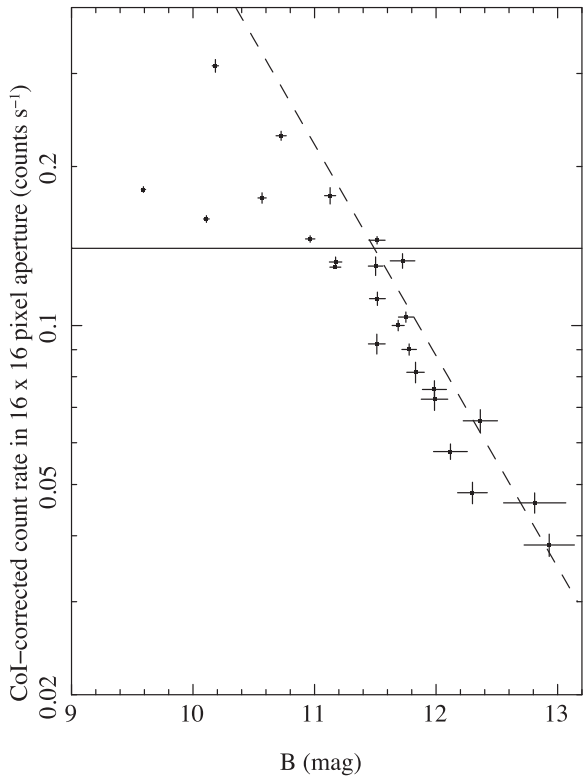

Figure 5. Data points show the read-out-streak count rates in 16 × 16-pixel apertures of *Tycho*-2 stars in full-frame *XMM*-OM *B*-band images after correction for coincidence loss in the MCPs (equivalent to R_i in equations 3 and 4) against *XMM*-OM *B* magnitude, derived from *Tycho*-2 photometry (equation 8). The dashed line shows the expected relationship. The solid line shows a count rate of 0.14 counts s^{-1}, below which saturation effects are not important.

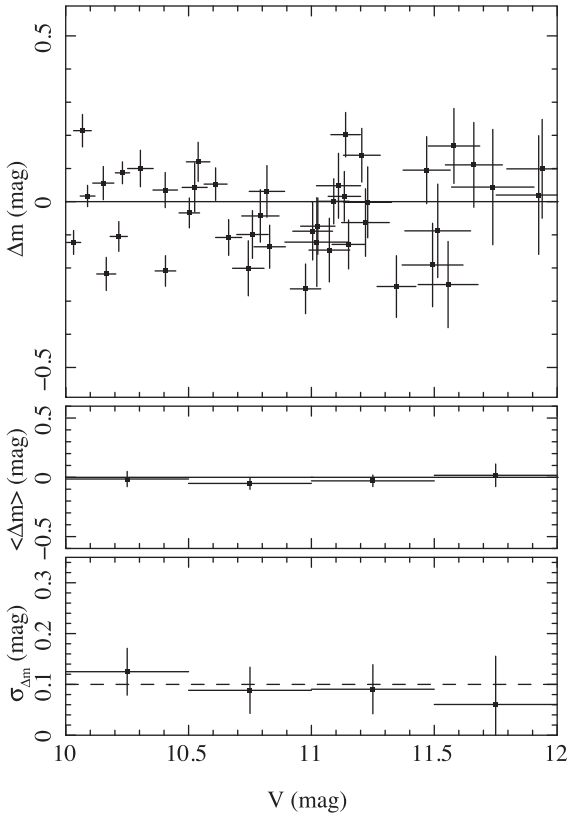

Figure 6. Top panel: differences Δm between the *V* magnitudes obtained from *Tycho*-2 and the *V* magnitudes obtained from the coincidence-loss-corrected count rates of the *XMM*-OM read-out streaks. Uncertainties are the quadrature sums of the errors on the count rates and the *Tycho*-2 magnitudes. Middle and bottom panels: mean and dispersion of Δm, respectively, in 0.5-mag bins. The dashed line in the bottom panel shows the best-fitting dispersion, $\sigma_{\Delta m} = 0.10$, over the full $10 < V < 12$ mag interval shown.

counts s^{-1}. Fig. 5 shows the coincidence-loss-corrected count rates for the *B* band compared to *B* magnitudes derived from *Tycho*-2 photometry. There are fewer *B* measurements, and the *Tycho*-2-derived *B* magnitudes have larger uncertainties than those for the *V* band. In addition, read-out streaks typically have larger statistical uncertainties in *B* than in *V* because *XMM*-OM *B* images typically have higher background levels than *V* images. Consistent with the findings from *V*-band photometry, saturation effects associated with the MCPs are only seen for $R_i > 0.14$ counts s^{-1}.

4.1 Photometric scatter

We now examine the scatter of the read-out-streak photometry measurements with respect to the *Tycho*-2 photometry to estimate the level of photometric accuracy that can be achieved for *XMM*-OM using read-out streaks. For UVOT, Page et al. (2013) found that systematic errors limit the photometric accuracy of read-out-streak photometry to 0.1 mag.

The top panels of Figs 6 and 7 show the differences between the read-out-streak and *Tycho*-2-derived magnitudes (Δm) for the individual stars in *V* and *B*. The uncertainties on Δm have been computed by adding in quadrature the statistical uncertainty on the read-out-streak photometry with the magnitude uncertainty given in the *Tycho*-2 catalogue. The *V* data in Fig. 6 are of higher quality than the *B* data in Fig. 7, both in terms of the precision of the individual measurements, and in the number of measurements. We have used the method of Maccacaro et al. (1988) to derive from these measurements in 0.5-mag bins, maximum-likelihood estimates of the mean and intrinsic standard deviation of the distribution of Δm, which we have assumed to be Gaussian. The middle panels of Figs 6 and 7 show the means, $\langle \Delta m \rangle$, and the bottom panels show the intrinsic standard deviations $\sigma_{\Delta m}$. The values of $\langle \Delta m \rangle$ are all consistent with 0, and no systematic trends are evident with magnitude. The individual values of $\sigma_{\Delta m}$ are less well determined. For the *V* band, applying the Maccacaro et al. (1988) method over the full range of magnitudes we obtain $\langle \Delta m \rangle = -0.025 \pm 0.025$ and $\sigma_{\Delta m} = 0.10 \pm 0.02$. The individual values of $\sigma_{\Delta m}$ obtained in 0.5-mag bins in both *V* and *B* bands are all consistent with $\sigma_{\Delta m} = 0.10$, which represents the level of systematic uncertainty that must be added in quadrature to the statistical uncertainties to reproduce the distribution of Δm. Thus photometry obtained from read-out streaks should be considered to have a systematic uncertainty of 0.1 mag, in addition to the statistical uncertainty. It is interesting to note that this level of systematic error, 0.1 mag, is identical to that derived for UVOT read-out-streak photometry by Page et al. (2013).

4.2 Brightness limits for images that are not in full-frame mode

From Figs 4 and 5 we identified a bright limit of $R_i = 0.14$ counts s^{-1} for read-out streaks in full-frame *XMM*-OM imaging, beyond

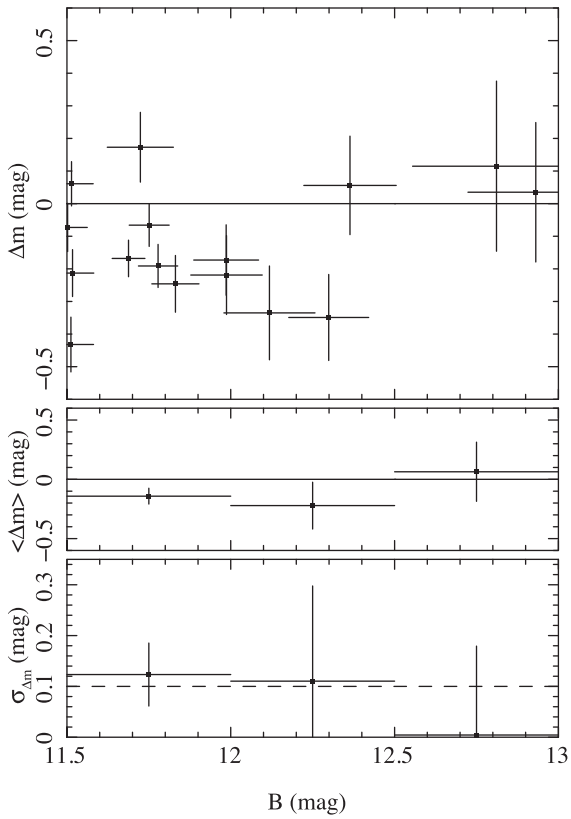

Figure 7. Top panel: differences Δm between the B magnitudes obtained from *Tycho*-2 and the B magnitudes obtained from the coincidence-loss-corrected count rates of the *XMM*-OM read-out streaks. Uncertainties are the quadrature sums of the errors on the count rates and the *Tycho*-2 magnitudes. Middle and bottom panels: mean and dispersion of Δm, respectively, in 0.5-mag bins. The dashed line in the bottom panel corresponds to a dispersion of 0.1 mag.

which saturation of the MCPs degrades the photometry. Different window configurations correspond to different frame times, and so different exposure-time ratios, S, according to equation (1). For full-frame imaging the frame time is 11.0388 ms, corresponding to $S = 9054$. The maximum acceptable count rate will scale inversely with S, so for an arbitrary frame time the bright-limit count rate for read-out-streak photometry is

$$R_{\max} = \frac{1268}{S}. \quad (9)$$

5 A DEMONSTRATION OF READ-OUT-STREAK PHOTOMETRY: THE NEAR ULTRAVIOLET EVOLUTION OF RR TELESCOPII

The Nova RR Telescopii is a symbiotic binary that underwent a nova outburst in 1944. In optical radiation, it has been slowly dimming ever since (Kotnik-Karuza et al. 2006). Between 1978 and 1995, its UV flux declined by a factor of 2–3, depending on wavelength (Nussbaumber & Dumm 1997). Shortwards of 1500 Å, the UV flux of RR Tel is thought to be dominated by the central star, while longwards of 1800 Å the UV flux is likely to be dominated by nebular emission (Nussbaumber & Dumm 1997). In a study of the X-ray and UV emission from RR Tel, based on an *XMM–Newton* observation taken in 2009, González-Riestra, Selvelli & Cassatella (2013) show that the 2009 *XMM*-OM photometry through the UVW2 and UVM2 filters are consistent with an extrapolation of the exponential decay seen in *International Ultraviolet Explorer* (*IUE*) data between 1978 and 1995. However, González-Riestra et al. (2013) describe the *XMM*-OM UVW1 photometry as uncertain, because it is subject to a large degree of coincidence loss. Indeed, in the *XMM*-SUSS 2.1 catalogue, there is no UVW1 magnitude for this source because it is flagged as being too bright for a reliable photometric measurement in UVW1. This is unfortunate, because it can be seen in González-Riestra et al. (2013) that the *IUE*-based photometry corresponding to the UVW1 filter is of a higher statistical quality than the photometry corresponding to UVW2 or UVM2. Using the read-out-streak technique, we are now able to derive valid UVW1 photometry from the 2009 *XMM–Newton* observation of RR Tel, and so can examine the UV photometric evolution over a 31-yr time base.

Photometry was derived from the 2009 *XMM*-OM UVW1 observation using the read-out-streak technique described here. The read-out streak is present in three of the five sub-exposures used to image the field around RR Tel, and is detected in all three sub-exposures with signal-to-noise ratios of between 46 and 48. Thus, the uncertainty on the photometry derived from the read-out streak is dominated by the 0.1-mag systematic term described in Section 4.1.

IUE large aperture, low-resolution spectra, reduced using the New Spectral Image Processing System (NEWSIPS; Nichols & Linsky 1996), were retrieved from the Mikulski Archive for Space Telescopes. UVW1 photometry was synthesized from the *IUE* spectra by integrating the product of *IUE* flux and the *XMM*-OM UVW1 response curve. The UVW1 passband extends further to the red than the spectral coverage of *IUE*, which ends at 3350 Å. In order to correct the *IUE* synthesized photometry for the missing red flux, we made use of a *Hubble Space Telescope* (*HST*) Space Telescope Imaging Spectrometer (STIS) observation of RR Tel from 2000, which provides full spectral coverage throughout the UVW1 passband. From the STIS data, we determine that the photometry of RR Tel synthesized only to 3350 Å is 0.12 mag fainter than the photometry synthesized over the full bandpass.

The statistical uncertainties on the UVW1 photometry synthesized from *IUE* spectra were initially propagated from the statistical uncertainties contained within the NEWSIPS spectral files. Examination of the scatter of the photometric data suggests that these uncertainties are too small. In particular, the rms of the UVW1 photometry derived from four *IUE* observations taken within a single day, 1994 May 7, is observed to be 0.13 mag, whereas the statistical uncertainties derived from the spectra are only 0.01 mag. Therefore, we have adopted 0.13 mag as the statistical uncertainty on the *IUE*-derived photometry.

Fig. 8 shows the *XMM*-OM UVW1 photometry together with the corrected, synthesized UVW1 light curve from *IUE*. We have not included the photometry derived from the *HST* STIS observation because this was obtained from a much smaller aperture (0.2 arcsec) than the *IUE* or *XMM*-OM photometry, and the spatial extent of the nebula is not known. The dashed line shows the best-fitting exponential decay model to the *IUE* and *XMM*-OM UVW1 photometry. From the fit, we derive an e-folding time of 19.4 ± 1.2 yr, which is somewhat shorter than the UVW1 e-folding time of 24 ± 1 yr derived by González-Riestra et al. (2013), but consistent with the e-folding times they derived for the shorter-wavelength UVW2 and UVM2 bands, which were 23 ± 5 and 21 ± 2 yr, respectively.

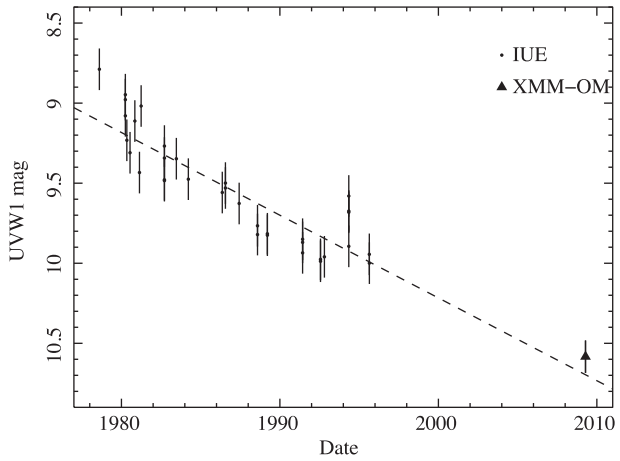

Figure 8. Light curve of RR Tel in the UVW1 bandpass, using read-out-streak photometry from *XMM*-OM and synthesized UVW1 photometry from *IUE*. The dashed line shows the best-fitting exponential dimming model, which corresponds to an e-folding time of 19.4 yr.

6 A SUPPLEMENTARY CATALOGUE OF PHOTOMETRY FOR BRIGHT *XMM*-OM SOURCES

The *XMM*-SUSS[7] is a catalogue of sources detected in *XMM*-OM images and consists of astrometric, photometric, and morphological information together with quality flags to appraise the user of the validity of the measurements (Page et al. 2012). The latest release of the catalogue, *XMM*-SUSS 2.1,[8] contains more than 4.3 million unique optical and UV sources. Sources that exceed a threshold of 0.97 counts per frame in a given band are deemed too bright for reliable photometry in that band. In such cases, magnitudes are not provided in the catalogue and quality flags indicate the bands for which the source is too bright. The read-out-streak photometry method that has been described in this paper permits photometry of sources up to 1.5 mag brighter than this threshold, and therefore offers the possibility to recover some of the missing photometry for these bright sources. We have therefore used read-out-streak photometry to produce a catalogue of photometric measurements for bright sources to form a supplement to the main *XMM*-SUSS 2.1 catalogue. In the following sub-sections, we describe how we constructed the supplementary catalogue and describe its basic properties.

6.1 Construction of the catalogue

A pipeline was constructed to measure read-out streaks in *XMM*-OM images and match them to stars in the *XMM*-SUSS that were too bright for their photometry to be measured from the direct image. Such sources can be identified in the *XMM*-SUSS 2.1 catalogue through having quality flag number 11 (with numerical value of 2048) set in the QUALITY_FLAG column[9] corresponding to the affected filter(s). As for the *XMM*-SUSS, each individual *XMM–Newton* pointing, corresponding to a unique observation identification number is treated independently in the supplementary catalogue. For each *XMM–Newton* observation containing one or more saturated stars, we retrieved the standard *XMM*-OM source-list and modulo-8-corrected raw-image products from the ESA *XMM–Newton* Science Archive (XSA). Read-out streaks were measured from the images using the software developed by Page et al. (2013), with bad pixels masked using the standard *XMM*-OM calibration file[10] from the CCF. The columns containing read-out streaks were then matched to the columns containing saturated stars in the source-lists. For *XMM*-OM observations carried out in the default imaging mode (also known as 'Rudi-5' mode) in which five separate images are taken in a mosaic pattern to form a full-field image, the read-out streaks often cross multiple images, but the saturated star is typically found in only one. Therefore, the pipeline merges the individual source-lists prior to matching the read-out streaks to stars.

It is possible for more than one bright source to land on the same column within the *XMM*-OM image, particularly in crowded fields near to the Galactic plane, and in such cases multiple stars will contribute to the read-out streak, invalidating the photometry. We have discarded read-out-streak photometry for saturated stars in which one or more additional stars with count rates of >20 counts s^{-1} are found in the source-list within eight raw columns of the saturated star. The threshold of 20 counts s^{-1} corresponds to a maximum contaminating contribution of 8 per cent to the read-out streak of a saturated star.

We also identified cases in which two read-out streaks are detected in close proximity (within 24 raw columns), and discarded any corresponding read-out-streak photometry. Although this condition occasionally identifies cases of bright sources lying on close-enough columns that their read-out-streak photometry is affected, its main purpose in the pipeline is to identify stars that are far too bright for read-out-streak photometry but cannot be identified as such from the count rates of their read-out streaks (see section 5.1 of Page et al. 2013). Visual screening was used to reject other examples of such stars that are too bright for read-out-streak photometry, but which were not identified by their count rates or by the apparent proximity of multiple read-out streaks.

During the construction of the catalogue, it became evident that in extremely crowded star fields, background determination becomes very challenging. In extreme cases, the column-by-column background as determined in the pipeline by the algorithm described in Section 3.3 shows large systematic deviations that compromise the read-out-streak measurement. From visual examination of the background curves for fields containing different densities of sources, we have chosen a threshold of 2000 sources per full-frame *XMM*-OM

Table 2. Source statistics for the supplementary catalogue. The mean magnitudes for the sources in each filter are Vega magnitudes in the *XMM*-OM photometric system.

Filter	Number of saturated objects in *XMM*-SUSS 2.1	Number of objects in supplementary catalogue	Mean magnitude in supplementary catalogue
V	978	258	11.06
B	1670	460	12.34
U	1252	440	11.35
UVW1	675	329	10.28
UVM2	88	53	8.80
UVW2	9	4	7.65

[7] http://www.cosmos.esa.int/web/xmm-newton/om-catalogue
[8] http://www.ucl.ac.uk/mssl/astro/space_missions/xmm-newton/xmm-suss2
[9] See http://www.ucl.ac.uk/mssl/astro/space_missions/xmm-newton/xmm-suss2 for details of the *XMM*-SUSS 2.1 quality flags.

[10] Calibration file OM_BADPIX_0005.CCF.

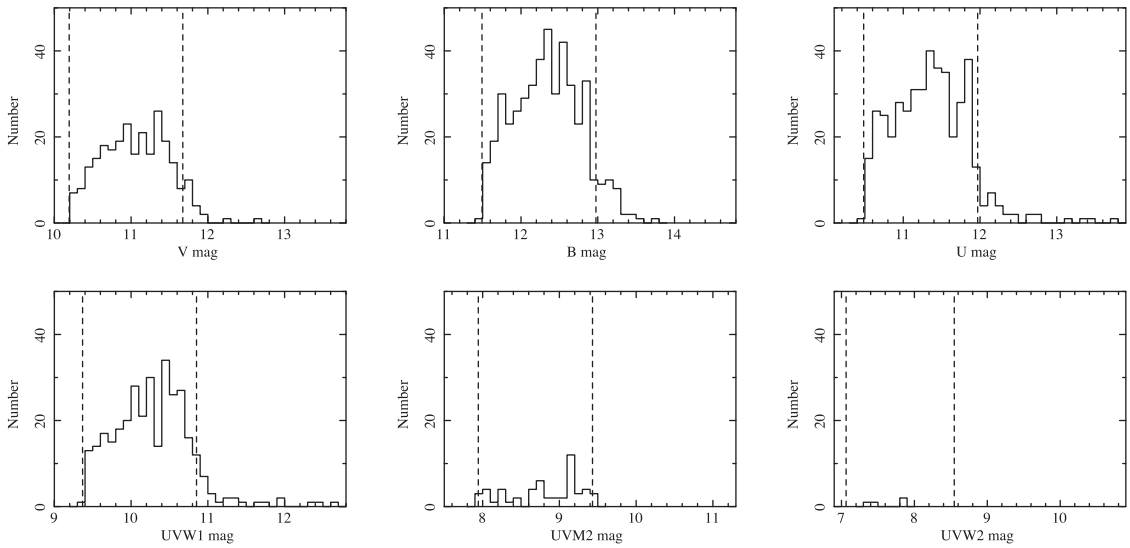

Figure 9. Magnitude distributions of the supplementary catalogue entries for the six passbands used in the *XMM*-SUSS. The two dashed lines in each panel indicate the bright limits for read-out-streak photometry and aperture photometry.

image; where the field is imaged through a sequence of windowed exposures as in the default imaging mode, the sources are summed over all the exposures. We have discarded read-out-streak photometry derived from images that exceed this threshold.

6.2 Properties of the catalogue

Basic statistics for the supplementary catalogue are presented in Table 2. Overall, valid photometry is recovered for 50 per cent of the UV measurements and 30 per cent of the optical measurements, which are saturated in *XMM*-SUSS 2.1, using read-out streaks. The magnitude distributions for the supplementary catalogue entries in the six passbands are shown in Fig. 9. The dashed lines correspond to the nominal brightness limits for read-out-streak photometry and aperture photometry for full-frame images early in the mission, so we would expect the vast majority of sources to lie within the 1.5-mag interval between the two lines. A small number of sources are found to be brighter than the left dashed line because the bright limit has increased slightly (by up to 0.2 mag depending on filter) over the course of the *XMM–Newton* mission as the *XMM*-OM detector has aged. Some spill-over of sources beyond the right dashed line is expected because these are the faintest read-out-streak measurements and hence have the largest photometric errors. However, a tail of sources is seen in several passbands between 0.5 and 2 mag fainter than the right dashed line. Stars with these magnitudes should be well below the 0.97 counts per frame saturation limit of *XMM*-SUSS 2.1 by which they were selected for read-out-streak measurement. Therefore, we have visually inspected each of the sources that are more than 0.5 mag fainter than the dashed lines in Fig. 9, of which there are 23 in total. We found that in 12 cases the bright sources were on edge of the image, such that the count rate measurement in *XMM*-SUSS 2.1 is flawed. The read-out-streak photometry appears to be correct in 11 of the 12 cases. In a further five cases, the sources are bright galaxies, with the *XMM*-SUSS 2.1 measurement including counts from a much larger region than the standard point-source aperture. In these cases, the read-out-streak photometry provides reasonable estimates for the nuclear regions of these galaxies. The remaining six cases include two spurious scattered light features that have been treated as extended sources in *XMM*-SUSS 2.1, 2 sources in which the presence of bright sources in the neighbouring columns has caused problems with the local background estimate for the read-out-streak photometry, and two sources in which Flag number 11 appears to have been set incorrectly; in both these latter cases, the aperture photometry from the image agrees with the read-out-streak photometry. Overall the great majority of read-out-streak measurements appear to be correct among these apparently outlying points, so the tail of faint read-out-streak magnitudes is not a cause for concern.

6.3 Catalogue access

The supplementary catalogue is available as a fits file via the MSSL *XMM*-SUSS2 web pages[11] and will be available from the ESA XSA.[12]

7 CONCLUSIONS

We have shown that read-out streaks in *XMM*-OM images can be used for photometric measurements of stars that are brighter than the coincidence-loss limit for normal aperture photometry. The study is based on *XMM*-OM *V*- and *B*-band measurements of stars in the *Tycho*-2 catalogue. We find that the recharge time-scale for the pores of the MCPs in *XMM*-OM is $5.5\pm0.1 \times 10^{-4}$ s, which sets the bright-source limit for read-out-streak photometry to be 1.5 mag brighter than the limit imposed by coincidence loss in the CCD in full-frame images. We find that systematics and unaccounted errors limit the precision of the read-out-streak photometry to 0.1 mag. As a demonstration, we have derived UVW1 photometry of the symbiotic nova RR Tel using read-out streaks, and compared it to photometry derived from earlier *IUE* observations. We have used the read-out-streak method to construct a supplementary catalogue of photometry for sources that were too bright for photometric measurement in the *XMM*-SUSS 2.1 catalogue. Using this method, photometry is recovered for 50 per cent of the UV measurements that exceeded the *XMM*-SUSS 2.1 bright limit.

[11] http://www.mssl.ucl.ac.uk/www_astro/XMM-OM-SUSS/suss2_1/
[12] http://www.cosmos.esa.int/web/xmm-newton/xsa

ACKNOWLEDGEMENTS

This work is based on observations obtained with *XMM–Newton*, an ESA science mission with instruments and contributions directly funded by ESA Member States and NASA.

REFERENCES

ESA 1997, The Hipparcos and Tycho Catalogues, ESA SP-1200
Fordham J. L. A., Bone D. A., Read P. D., Norton T. J., Charles P. A., Carter D., Cannon R. D., Pickles A. J., 1989, MNRAS, 237, 513
Fordham J. L. A., Moorhead C. F., Galbraith R. F., 2000a, MNRAS, 312, 83
Fordham J. L. A., Kawakami H., Michel R. M., Much R., Robinson J. R., 2000b, MNRAS, 319, 414
González-Riestra R., Selvelli P., Cassatella A., 2013, A&A, 556, A85
Høg E. et al., 2000, A&A, 355, L27
Kotnik-Karuza D., Friedjung M., Whitelock P. A., Marang F., Exter K., Keenan F. P., Pollacco D. L., 2006, A&A, 452, 503
Kuin N. P. M., Rosen S. R., 2008, MNRAS, 383, 383
Maccacaro T., Gioia I. M., Wolter A., Zamorani G., Stocke J. T., 1988, ApJ, 326, 680
Mason K. O. et al., 2001, A&A, 365, L36
Nichols J. S., Linsky J. L., 1996, AJ, 111, 517
Nussbaumer H., Dunn T., 1997, A&A, 323, 387
Page M. J., Carrera F. J., Stevens J. A., Ebrero J., Blustin A. J., 2012, MNRAS, 416, 2792
Page M. J. et al., 2013, MNRAS, 436, 1684
Pickles A. J., 1998, PASP, 110, 863
Roming P. W. A. et al., 2005, Space Sci. Rev., 120, 95
Skrutskie M. F. et al., 2006, AJ, 131, 1163
Talavera A., 2011, Technical Report XMM-SOC-CAL-TN-0019 issue 6.0, XMM–Newton Optical and UV monitor (OM) Calibration Status. ESA, Noordwijk, Available at: http://xmm2.esac.esa.int/docs/documents/CAL-TN-0019.pdf

This paper has been typeset from a TEX/LATEX file prepared by the author.